FRACTIONAL SNOW COVER MAPPING THROUGH POLYTOPIC VECTOR ANALYSIS OF MODIS SPECTRAL REFLECTANCE

A Thesis

by

YANG JU

Submitted to the Office of Graduate and Professional Studies of
Texas A&M University
in partial fulfillment of the requirements for the degree of

MASTER OF SCIENCE

Chair of Committee,	Andrew Klein
Committee Members,	Michael Bishop
	Sorin Popescu
Head of Department,	David Cairns

May 2017

Major Subject: Geography

ABSTRACT

Snow cover plays an important role in the Earth's climate systems. Accurately estimating snow cover is beneficial for predicting the runoff from snowmelt. Fractional Snow Cover (FSC) mapping computes the fraction of snow within a pixel of a remote sensing imager and provides a more precise snow cover extent estimate compared to binary comparing to binary identification of a pixel as snow or not. Linear mixture analysis has been commonly adopted to map FSC and multiple algorithms have been developed using this method. Polytopic Vector Analysis (PVA) is performed as an alternative to linear mixture analysis. PVA has some inherent advantageous over the standard linear unmixing method, which include that the generic PVA approach guarantees each endmember fraction falls within a physically realistic range (0 to 1 or 0 to 100%) and PVA automatically selects endmembers in an objective manner.

This study investigates the feasibility that applying PVA in mapping FSC. The PVA algorithm was developed in python, and was tested by using MODIS atmospherically-corrected spectral reflectance to determine snow-cover fraction. Reference fractional snow cover maps created from 30m-resolution Landsat images were used to assess the proposed method's performance. The PVA method showed a R^2 of 0.63 and RMSE of 0.12. This result is comparable with the MOD10 binary FSC product, but not as good as the MOD10 FSC product and Artificial Neural Network. However, as a parsimonious approach, PVA showed its potential for FSC mapping.

ACKNOWLEDGEMENTS

I would like to thank my committee chair, Dr. Klein, for his guidance of every step in detail of the project, and my committee members, Dr. Bishop, Dr. Popescu, for their interesting and informative courses in *Digital Image Processing* and *Advanced Remote Sensing*, respectively. I would also like to thank the Department of Geography at Texas A&M University for its great research environment and thank the GEOSAT center for providing the Virtual Machine and make my analysis more efficiently.

Thanks also go to my friends and colleagues and the department faculty and staff for making my time at Texas A&M University a great experience. In particular, I would like to thank Iliyana Dobreva for her assistance in collecting data and providing feedbacks.

Finally, thanks to my mother and father for their encouragement and support.

CONTRIBUTORS AND FUNDING SOURCES

Contributors

This work was supervised by a thesis committee consisting of Dr. Klein and Dr. Bishop of the Department of Geography and Dr. Popescu of the Department of Ecosystem Science and Management. The data analyzed for Chapter III was provided by Iliyana Dobreva and Dr. Klein. All other work conducted for the thesis was completed by the student.

Funding Sources

There are no outside funding contributions to acknowledge related to the research and compilation of this document.

TABLE OF CONTENTS

Page

LIST OF FIGURES

Page

LIST OF TABLES

Page

1. INTRODUCTION

1.1. Importance of Snow Cover Research

The presence of snow on the Earth plays a significant role over a wide range of spatial and temporal scales. It interacts with the natural environments and human both locally and regionally (Rees et al. 2005). Annual and interannual variations in snow cover are an important feedback mechanism to the Earth's climate and hydrology systems.

Snow cover is an important variable for climate as it can control the earth surface albedo (Nolin et al., 1997). The high albedo of snow in the visible and near infrared region of the electromagnetic spectrum makes the incoming solar radiation a high reflectance, which can influence the energy exchanged between ground and atmosphere (Arnfield, 2006). Snow cover provides the thermal insulation that can reduce the heat exchange between the ground and atmosphere (Rees et al. 2005).

Snow cover is also a key factor to the Earth's hydrology system. As frozen water, snow holds precipitation within the snowpack until released during snowmelt. Snowmelt runoff can lead to a flood when it releases rapidly in spring (Rango et al., 1998). Moreover, snow is also significant for its potential in water storage for drinking and irrigation (Rango, 1993). In fact, thirty percent of the Earth's land surface is covered by seasonally by snow (Dozier, 1989). Snow is essential for the supply of more than one sixth of the world's population that relies on the melt of snow and glacier for fresh water (Barnett et al., 2005).

Snow cover information can be included in hydrological models when predicting the runoff from snowmelt and the weather forecasting models (Dobreva et al., 2011). The quality of snow cover extent maps greatly influences the accuracy of climate modeling (Chokmani et al., 2013). Currently, ground observation networks remains the standard source for snow cover information. However, it is both labor intensive and financial consuming to use ground observations to obtain large scales snow cover extent information. Satellite images makes it possible to monitor snow cover at global scales.

There are various snow cover products available from different satellite data (Landsat, SPOT, MODIS, etc.). For climate modeling, snow cover extent should be produced at spatial resolutions of a few kilometers (Romanov et al., 2000). Difficulties may arise when the incorporated snow cover extent into climate models is inaccurate (Niu et al., 2007). Thus, accurate monitoring of spatial extent of snow cover by satellite data is imperative.

1.2. Study Purpose and Objectives

This study investigated the applicability of Polytopic Vector Analysis (PVA) of MODIS spectral reflectance to fractional snow cover mapping. To accomplish this goal, PVA code was originally developed in the Python Programming Languague (add citation for Python) and tested against existing PVA software using known mixtures of Polychlorinated Biphenyls (PCBs) from Murphy et al. (2014) to ensure it correct operation. Once, its performance was deemed acceptable The PVA code was then applied to analyze MODIS (Moderate Resolution Imaging Spectoradiomer) reflectance to map fractional snow cover for selected scenes over North America

PVA is a mixture analysis method first developed in the field of geological science. It is a multivariate technique based on a linear mixing model, involving resolution of oblique vectors as source composition, thus the term vector analysis was used employed in naming the technique instead of factor analysis, the more commonly used term in geology.. PVA has advantages over the standard linear unmixing method in that 1) it calculates the fractions in a realistic range (0-1 or 0 to 100%), and 2) it determines the endmembers in a more objective way.

Although PVA has been used extensively in multivariate mixture analysis in the filed of earth and environmental science, it is a relative new tool in remote sensing application (Nash et al., 2002). Its only prior known use in remote sensing was a vegetation study for analysis of Dixie Valley AVIRIS data within a small subset of study area (Johnson et al., 1998). However, to our knowledge PVA has not been applied to determination of fractional snow cover. Considering the similarity between mixed pixels of remote sensing imagery and multivariate mixture of environmental science, more exploration of the applicability of PVA in study is needed for remote sensing, especially in study of fractional snow cover.

This study used surface reflectance from seven MODIS bands. MOD09 is the MODIS atmospherically-corrected surface reflectance product that computed from the MODIS Level 1B land bands 1 – 7. The seven estimated land surface reflectance bands at 500 m spatial resolution were used in the study as inputs to produce the fractional snow cover. Landsat derived snow cover fractions were used as reference (Dobreva and Klein, 2011) to estimate mapping accuracy of PVA. Snow fractions calculated by

Artificial Neural Network (ANN) and MOD10 (Dobreva and Klein, 2011) were also compared with those computed from PVA to evaluate the performance of PVA.

2. LITERATURE REVIEW

2.1. Snow Cover Extent Mapping

Snow cover extent is a key factor in the Earth's climate and hydrology systems, as well as is of important for its economic and hazards effects (Rango, 1996, Roesch et al., 2001). In the past decades, progress has been made in snow cover extent mapping as remote sensing technology has developed. However, descriptive observations of snow can be dated back to early 18th century in Switzerland which was to underline stratigraphy snowpacks (Pielmeier and Schneebeli, 2003). *In situ* measurement was utilized to collect snow information through manual collections of snowpack information in the early year (Derksen and LeDreww, 2000). However, the practice of manual snow course survey was gradually replaced in the 1980s by networks of automated snow telemetry (SNOTEL) stations, which is capable of providing snow information in nearly real-time (Brown, 2009).

In situ measurements of snow cover, however, are criticized for being biased toward populated areas and for providing only localized data (Brown and Braaten, 1997). It is also difficult to manually collect consistent snow cover information under adverse weather conditions (Derksen and LeDrew, 2000). On the other hand, remote areas often lack meteorological observations or are not included in SNOTEL or similar automated networks that makes stationary measurements of regional snowfall characteristics inaccurate or incomplete as well (Koskinen et al., 1999). As technology advanced, satellite and airborne began to be utilized to measure snowfall with unprecedented

accuracy to the end of the 20th century (Brown, 2009; Robinson et al., 1993). The combination of ground-based observations and remote sensing products such as aerial photography, satellite and radar imagery are being increasingly used to measure snowfall characteristics (Cherry et al., 2007).

The high albedo of snow in visible and near infrared region of the electromagnetic spectrum coupled with its low reflectance in the short-wave infrared makes it readily distinguishable from other surface features in remote sensing images and hence make remote sensing a suitable and powerful tool to monitor snow cover area globally (Rees, 2005). In addition, as a convenient tool, remote sensing allows snow detection over remote and inaccessible areas for the snow cover is often prevalent in these regions (Nolin, 2010). Currently, there are two main methods for snow cover mapping from satellite data. One is binary classification of snow cover. This approach aims to distinguish each pixel in an image is snow or not typically by comparing the Normalized Differential Snow Index (NDSI) to a threshold which is set empirically (Dozier, 1989). Increasingly fractional snow cover mapping has been undertaken. This approach is an enhancement from the binary classification, which computes the fraction of snow within each pixel of a remote sensing image (Nolin, 2010).

2.2. Binary Classification

Binary (i.e., snow or not-snow) classification on snow cover mapping typically aims to determine if a pixel is snow or not based on Normalize Difference Snow Index (NDSI), which was originally developed for Landsat (Dozier, 1989). Snow reflects nearly 90% of the incoming solar radiation in the visible region of the electromagnetic

spectrum and is easily to be observed in true-color image (Dobreva, 2009). Remote sensing investigation uses the contrast that snow has the high albedo in the visible spectrum and a low albedo in the shortwave infrared range of the electromagnetic spectrum which while characteristic for snow is not typical for most land covers. NDSI applies this contrast to discriminate snow from other ground features (Dozier, 1989; Hall et al., 1995). This index is computed by constructing a normalized ratio between the reflectance in the visible and shortwave infrared (SWIR) rages of the electromagnetic spectrum:

$$NDSI = \frac{R_{VIS} - R_{SWIR}}{R_{VIS} + R_{SWIR}} \quad (1)$$

where R represents planetary reflectance in a visible band and a shortwave infrared band. For MODIS snow product, these are Terra MODIS band 4 (0.545 – 0.565 μm) and band 6 (1.628 – 1.652 μm). However, due to the failure of band 6 on Aqua, band 7 (2.105 – 2.155 μm) is often used as a replacement. NDSI ranges from -1 to 1. Historically, a pixel is identified as snow when the NDSI is above 0.4 in areas where forest canopy does not obscure the surface (Dozier, 1989; Hall et al, 1995). This NDSI greater than 0.4 threshold generally maps a pixel as snow cover when its snow fractions exceeds 50% (Hall et al., 2002). For snow in forests, Normalized Difference Vegetation Index (NDVI) is utilized in addition to NDSI. NDVI normalizes between the near infrared reflectance and visible reflectance.

$$NDVI = \frac{R_{NIR} - R_{VIS}}{R_{NIR} + R_{VIS}} \quad (2)$$

Klein et al. (1998) combined a snow reflectance model with a canopy reflectance model with a canopy reflectance model to identify snow covered forested areas when NDSI is below 0.4 but NDVI is above 0.1.

However, challenges arise when applying remote sensing on snow cover mapping. One of the most important obstacles is the tradeoff between the temporal and spatial resolution of satellite imageries. On one hand, when the spatial resolution is high, images are often not available on a daily basis for all of the Earth. For example, the Landsat ETM+ has a 30m resolution but its temporal repeat is 16 days, which is inadequate for monitoring to changes in snow cover and calculating snowmelt runoff.. On the other hand, when the temporal resolution is acceptable, the spatial resolution is often a limitation in mapping the snow cover as pixel sizes become large often on the order of hundreds of meters or more. The precision of snow cover maps produced using these imageries may not be very reliable. Therefore, an idea of sub-pixel classification of low or moderate resolution images has been proposed.

2.3. Fractional Snow Cover Mapping

Fractional snow covered area (FSC) is the fraction of snow cover in a pixel of a remote sensing image. FSC values are ranging from 0 to 1 or 0 to 100% of a pixel. For

areas that have patchy snow, such as near the snow line and in wind-scoured areas, the fractional area is often preferred as it can be more accurate over the binary classification in estimating total snow cover area for an area (Nolin, 2010)

2.3.1. Fractional Snow Cover Mapping based on NDSI

Salomonson and Appel (2002) developed an algorithm that estimating the subpixel snow fraction from MODIS using a linear relationship between FSC and NDSI. They employed 30m Landsat imagery as "ground truth" data to calculate the fraction of snow within each 500m MODIS imagery. Then the relationship between NDSI and MODIS snow fraction was developed over three different snow covered regions, including a snow-covered region in Alaska, a relatively flat region in Canada and a taiga region in Russia. The regression relationship created by these three regions were then tested over other areas and the overall results indicates that this developed relationship between fractional snow cover and NDSI is reasonably robust when applying locally and over large areas. This method can provide a mean absolute error less than 0.1 over the range from 0 to 1 in fractional snow cover.

The MOD10A1 (Terra) and MYD10A1 (Aqua) fractional products utilize an empirical relationship between fractional snow cover and the NDSI as well (Salomonson and Appel, 2002). The models have the form that:

MOD10A1

$$f_{SCA} = -0.01 + 1.45NDSI \text{ , where } NDSI = \frac{R_4 - R_6}{R_4 + R_6} \quad (3)$$

MYD10A1

$$f_{SCA} = -0.64 + 1.91NDSI \text{ , where } NDSI = \frac{R_4 - R_7}{R_4 + R_7} \quad (4)$$

The coefficients were determined by comparing MODIS scenes with Landsat ETM+ imagery using the method mentioned above. Although it is a well-constrained relationship between the NDSI and the fractional snow cover, the estimated fraction of snow can be erroneously low when applying on areas of forest canopy, as the approach measures only viewable snow cover.

2.3.2. Fractional Snow Cover Mapping based on Spectral Mixing

The other commonly used approach to compute the fraction of snow within pixel is spectral mixture analysis. The earliest study on mapping fractional snow-covered area utilized linear spectral mixture analysis method applied on hyperspectral imaging spectrometer data (Nolin et al., 1993; Nolin, 2010). Spectral mixture analysis requires that the sensor must be able to detect differences between different spectral reflectance characteristics of the various land-cover elements within a remote sensing imagery, such as snow, vegetation, soil and water. Each of these land-cover elements is also referred as endmember. The endmember is an ideal and pure spectral signature of each ground type (Schowengerdt, 1997). For spectral mixture analysis, the sensor should have at least as many channels as endmembers in the image, and the recorded reflectance information should have non-redundant spectral reflectance values of each land-cover type (Sabol et al., 1992).

The spectral mixture analysis assumes that the reflectance of a pixel, which containing multiple endmembers is a linear combination of the reflectance values of each surface component weighted by its fraction in that pixel (Jensen, 2005).

$$\rho_i = \sum_{j=1}^{n} f_j \rho_{ij} + E_i \tag{5}$$

Where ρ_i is the pixel reflectance in spectral band i, f is the fraction of the jth endmember in the mixed pixel, n is the number of endmembers, ρ_{ij} is the reflectance of endmember j in spectral band i, and E_i is the error of the fit of the leaner model to the data.

The performance of spectral unmixing depends on the availability of accurate and complete endmembers. Extensive studies of snow cover mapping have used this method (Painter et al., 1997; Painter et al., 2003; Painter et al., 2009; Simpson et al., 1998; Simpson et al., 2001). These studies differ in the methods used to collect endmembers and the endmembers selected to map the fractional snow cover by the different algorithms.

Painter et al. (1997) used mixture analysis to estimate sub-pixel snow-covered area and snow grain size from the AVIRIS data. They presented a technique that estimated snow-cover area and snow grain size simultaneously by optimization of mixture analysis with multiple snow endmembers. Mixture models with vegetation, rock and shade endmembers were applied with each snow endmember. The snow fraction for

each pixel was then estimated by the model with least mixing error. Results in this study demonstrated that the technique is accurate at estimating sub-pixel snow covered area. Painter at al. (1997) tested this method on a 5 April 1994 AVIRIS scene of Mammoth Mountain, California. Their results indicated that the technique of multiple snow endmembers gives snow covered area results equivalent to those from high spatial resolution aerial photographs with a well modeled linear regression relationship ($photographic = 0.0242 + 0.962 AVIRIS$; $r^2 = 0.981$). Painter el at. (2003, 2009) developed another model for retrieval sub-pixel snow covered area and grain size from imaging spectrometer data. This model is called MEMSCAG (multiple endmember snow covered area and grain size), which can map snow and its grain size simultaneously using spectral mixture analysis coupled with a radiative transfer model. Multiple-end-member choices are also allowed for rock and vegetation to accommodate spatial heterogeneity of these land-cover types within an image. There is a spectral library that stores the end-member spectral reflectance curves, which are used in the optimization scheme by the spectral mixture model. The spectral mixture selects the best fit for each and computing the varying fractions of each end-member for each pixel model by analyzing the multiple end-members. In addition to the estimated viewable fraction of snow-covered area, the model also reports the best-fit snow grain size, which is then used to estimate snow albedo. The MEMSCAG approach has been extended to MODIS with MODSCAG (Painter et al. 2009). Assessment of the MODSCAG snow-cover mapping method claims a root-mean-square (RMS) error of 5%.

Simpson et al. (1998) proposed a procedure to accurately separate snow and clouds from clear land in a terrestrial scene, identify mixed pixel class and assign percentage composition (snow, cloud, and land) for pixels in this class using a linear mixing model. This proposed method was applied on AVHRR (Advanced Very High Resolution Radiometer) data and the results showed accuracy about 97% when evaluating the classification skills based on a statistical comparison with SNOTEL observations. In the year 2001, Simpson and McIntire developed another method for retrievals of areal extent of snow cover. They used a feed-forward neural network (FFNN) to classify individual images and a recurrent neural network to classify sequences of images. Mixed-pixel classification was supported by the continuous outputs of the NN, which was also combined with a linear mixing model. Results applied on AVHRR data showed classification accuracy of 94% for feed-forward NN and 97% for recurrent NN respectively when validation with independent *in-situ* data. Dobreva et al. (2011) developed an algorithm for fractional snow cover mapping from MODIS reflectance using Artificial Neural Network (ANN). This machine learning method was developed and tested using MODIS and Landsat data on scenes obtained over North America, with comprehensive land cover types. A multilayer feed-forward ANN was trained in this study through back propagation to estimate FSC using MODIS surface reflectance, NDSI, NDVI and land cover as inputs. The developed method presented a RMSE of 12% of training scenes, and 14% of independently test scenes, which are both comparable favorably with the standard MODIS FSC snow product of Salomonson and Appel (2004).

2.4. Polytopic Vector Analysis

Polytopic Vector Analysis (PVA) was first developed for mixture analysis in geological sciences. It is a multivariate technique based on a linear mixing model and has a long established use, but has rarely been applied in remote sensing. The name PVA follows directly from the terminology of Imbrie (1963) and Full et al. (1981, 1982). The eigenvector decomposition model was referred as factor analysis when it resolved in terms of orthogonal axes, and was referred as vector analysis when it resolved in terms of oblique vectors, according to Imbrie (1963). PVA utilizes oblique vectors to resolve source composition, thus the term vector analysis was used instead of factor analysis. The roots of PVA are in principal components analysis, pattern recognition, linear algebra, and mathematical geology. Its development in mathematical geology can be dated back to the early 1960s (Murphy et al., 2014). A series of software were then developed (Manson and Imbrie, 1964; Klovan and Imbrie, 1971). Klovan and Imbrie (1971) developed a FORTRAN-IV program for large-scale Q-mode factor analysis and factor scores calculation. The Q-mode factor analysis is a multivariate procedure for studying relationships among items. The program they designed was called CABFAC, Calgary and Brown Factor Analysis, and at the time could handle up to 1500 items on a moderate-sized computer. This was then quickly became the most commonly used multivariate analysis algorithm in geoscience (Murphy et al., 2014). William Full subsequently made crucial contribution to the PVA algorithm (Full et al., 1981, 1982).

Miesch built on Imbrie's oblique vector rotation methods and developed the variable-by-variable goodness-of-fit criteria. Miesch (1976) demonstrated the

application of the extended Q-mode method, which was originally developed by Klovan and Imbrie (1971) to four problems in igneous petrology. Instead using the the Kolvan and Imbrie method, Miesch (1976) modified the approach to include a data transformation that transformed the original data into constant row-sum data. This assures that the composition scores (end-member compositions) are unity for each sample and the composition loadings (mixing or unmixing proportions) sum to unity for each sample. Miesch also demonstrated that the resultant model was in reasonable accord with geologic observations. Full et al. (1981, 1982) developed the DENEG approach to PVA, which stands for DElete NEGatives, to allow endmembers to be resolved without a priori knowledge of their composition and without need fora training data set. They introduced a modification of the Q-Mode unmixing algorithm (Klovan and Miesch, 1976) wherein an iterative procedure was developed to locate feasible end members not captured within a dataset. The algorithm that locates the endmembers was called the DENEG procedure. It does so by making an "edge-adjustment" of the mixing polytope based on negative mixing proportions, followed by a "vertex adjustment" based on negative composition scores.

2.4.1. Advantages of Polytopic Vector Analysis

PVA has some advantages over the standard linear unmixing method when applied to determining fractional snow cover. First, the standard linear spectral unmixing determines the snow cover percentages of individual endmembers may be physically unrealistic (e.g. endmember fractions that are negative or exceed 1 or 100%) while the PVA calculated fractions of the individual endmembers are constrained to sum to unity.

According to Miesch (1976), the Q-mode factor analysis is more easily to be interpreted because that the endmember composition loadings sum to unity.

Second, PVA can be used to directly determine the endmembers in a more objective way than the linear spectral unmixing in that it can determine the endmembers during the computing process automatically while the latter method typically selects the endmembers beforehand by user input. Full et al. (1982) demonstrated that the QMODEL method could determine the endmember without *a priori* knowledge.

2.4.2. Polytopic Vector Analysis in Remote Sensing Study

As described above, PVA was a method developed in geological science. Although PVA has been used extensively in multivariate mixture analysis in the earth and environmental science, it is a relative new tool in remote sensing application (Nash et al., 2002). It has been used in a vegetation study for analysis of Dixie Valley AVIRIS data within a small subset of study area (Johnson et al., 1998). This paper presents am initial result of spectral unmixing experiments, which was taken in the place of Dixie Valley, Nevada. PVA was used in this study to resolve parameters including the number of endmembers contributing to the mixture, the spectral composition of each endmember, and the relative proportion of each endmember in each sample.

The study of Johnson et al. (1998) was the first application of PVA to hyperspectral data, and it shows a potential to apply PVA onto remote sensing study. However, while it has been occasionally used in remote sensing afterwards, it has not been applied to snow remote sensingstudy before. From Johnson's study, it can be seen that the

PVA is capable of differentiating endmembers from remote sensing spectral data and thus it is possible to be applied on unmixing snow cover extent from other ground features. Therefore, as a potential tool in remote sensing, PVA needs more exploration of its applicability of remote sensing, and also in studies of fractional snow cover.

3. METHODOLOGY

3.1. Polytopic Vector Analysis (PVA)

As described in the previous section, Polytopic Vector Analysis (PVA) is one unmixing approaches that was originally developed for analysis of mixtures in the geological sciences. It aims to analyze the source compositions and their corresponding proportions in a mixture. The situation of a pixel in remote sensing image is akin to that of a mixture. For moderate resolution remote sensing data such as from MODIS, a pixel typically contains more than a single type of ground features. However, it is hard to determine the specific kind and corresponding percentage of each land cover on a sub-pixel level. Since PVA is designated to solve a similar problem, it is possible to apply the technique on analyzing the mixed pixel problem in remote sensing data and determine the proportion of the snow cover within each pixel.

The general principle of PVA is to apply a set of mathematic procedures on the mixture dataset to determine: (1) the composition of the end-members and (2) the relative proportions of each end-member in each pixel. The first task of PVA is to reduce the dimensionality of the dataset to extract the data which has the most useful information and make the computation easier than working on the whole dataset. Then endmembers are searched in the reduced dimension space by an iterative process. When the endmembers are determined, the proportions can also be determined. The detailed steps of PVA are detailed below:

3.1.1. Data Transformation

The equal vector length transform is often used in multivariate analysis of chemical data. It can force each of the sample vectors to have equal Euclidean length. Considering MODIS spectral reflectance data, this transformation can ensure the resultant proportion of each endmember within a pixel sums to unity. If all vectors have equal length, the differences between samples can be a function only of the angles between samples. The similarity and differences between samples can be expressed as a similarity matrix of cosines. The cosine between two identical samples is 1.0 while that between two completely different samples is 0.0. The procedure to conduct equal vector length transformation is documented in equations 6 – 8.

$$x'_{ij} = (x_{ij} - x_{\min}) / (x_{\max j} - x_{\min j}) \tag{6}$$

$$y_i = \frac{1}{(\sum_{j=1}^{n} x'^{\,2}_{ij})^{1/2}} \tag{7}$$

$$X'' = YX' \tag{8}$$

Equation 6 is a range transform for the input data, also known as minimum /maximum transform. In equation 6, x is the input MODIS spectral reflectance data, a *pixel *band* matrix, i is the number of row, and j is the number of column. The Range transform results in matrix where the maximum value in a column to be 1.0 and the minimum to be 0.0. In remote sensing images, the reflectance values of pixels can be of great variability from one to another, especially from between different columns in this

case. The range transformation eliminates this large difference among reflectance values of different MODIS bands, but still captures the variability within each band. The advantages of range transform are that: (1) there is no implication of a standard normal distribution; and (2) all the values are nonnegative as they fall in range 0.0 – 1.0.

Equation 7 and 8 are the steps of equal vector length transformation. X' is the range transform matrix. Y is a matrix whose diagonal elements y_i are defined by equation 7, y_i equal to the inverse of the square root of the sum-of-square along rows of X', and off-diagonal elements are zero. For MODIS imagery in this study, each pixel has seven reflectance values for each pixel, which is also termed a vector in this study. When performing the equal vector length transformation, the difference among samples can be represented by the $\cos\theta$ value between one sample and another.

3.1.2. Eigenvector Decomposition

Eigenvector decomposition is a mathematical procedure for reducing dimensionality of a data set. It is also the core mathematical operation in principle component analysis (PCA), which is most often accomplished by singular value decomposition (SVD) of the transformed matrix X''. Given a transformed matrix X'' composed of m rows and n columns, PCA can be completed through SVD of X'':

$$X'' = U\Lambda^{1/2}V' \tag{9}$$

Where U is the eigenvector matrix ($m \times k$) obtaining from a decomposition of $[X''][X'']^t$, V is the eigenvector matrix ($n \times k$) resulting from a decomposition of

$[X'']^t[X'']^t$, and Λ is the diagonal matrix of eigenvalues. $\Lambda^{1/2}$ is a diagonal matrix of the square root of the eigenvalues, which is referred as matrix S. For PCA, equation 9 is always expressed as the terms of principle components scores and loadings:

$$A = U\Lambda^{1/2} \tag{10}$$

$$F = V^t \tag{11}$$

Where A is termed as the loadings and F is the scores. In terms of fractional snow cover mapping, A is the fraction matrix for different land cover types, and F is the source composition matrix, which is the reflectance of different land cover at each MODIS band. A model resulted from reduced number of principle components can be represented as follow:

$$\underset{(m\times n)}{X''} = \underset{(m\times k)}{A''}\ \underset{(k\times n)}{F''} + \varepsilon \tag{12}$$

Where ε is the error or residual term. Given an error-free, noise-free matrix with $m \geq k$, $n \geq k$ resulting from k sources, only k eigenvectors and eigenvalues will be extracted. In our experience, if $k = 3$, the first eigenvector will account for a high percentage of the total variance of a an image. The second eigenvector is constrained to be mutually orthogonal to the first, and the third eigenvector is mutually orthogonal to the first two. The data set may be equivalently in this three-dimensional reference space without loss of information. In this study, the choice of number m k is made by calculation of the cumulative percentage variance. The reduced dimensional model should be able to

explain a large portion of information in the original dataset. So here 95% is used as the cutoff in determining the number of eigenvectors retained.

The process called polytope resolution is then conducted following the determination of number k. The first k columns of A'' was selected to form the reduced matrix A'' of size $m \times k$. Because $\hat{X}'' = A''F''$, F'' can be determined by matrix regression equation as follows:

$$F'' = (A''^T A'')^{-1} A''^T X'' \tag{13}$$

Matrix A'' may be irreversible so this equation is required to compute F''. Matrices A'' and F'' can then be transformed back to the original metric using the scaling functions described below in section 3.1.3.

3.1.3. Scaling Functions: Back- Calculation to Original Matric

The transformations used in section 3.1.1 allow for the optimization of the eigenvector decomposition, but it make it difficult for interpretation or evaluation of matrices A'' and F'' in terms of their scientific context. The transformation is helpful for matrices calculation while the original measurement metric is more suitable for evaluation and interpretation. Miesch (1976a) proposed a method that can translate the equation $\hat{X}'' = A''F''$ back to $\hat{X} = AF$, where double prime, as X'', indicates that a matrix has been equal length transformed. The mathematics is discussed as follows. The first step of back-calculation, as Miesch described, is definition of scale factor: s_k.

Given k retained eigenvectors, a $1\times k$ row vector of scale factors $s=\{s_k\}$ is defined as:

$$s_k=\frac{K-\sum_{j=1}^{n}x_{\min j}}{\sum_{j=1}^{n}(f_{kj}"(x_{\max j}-x_{\min j}))} \tag{14}$$

K is a constant that usually equals to100, the sum of each row. $f_{kj}"$ is the element of scores matrix. $x_{\max j}$ is the maximum value in the j th column of the original data matrix X, and $x_{\min j}$ is the minimum value in the j th column of the original data matrix X.

The elements in loadings matrices F' and F are calculated as:

$$f_{kj}^{'}=s_k f_{kj}^{"} \tag{15}$$

$$f_{kj}=f_{kj}^{'}(x_{\max j}-x_{\min j})+x_{\min j} \tag{16}$$

The elements of the back-calculated loadings matrices A' and A are calculated as:

$$a_{ik}^{'}=\frac{a_{ik}^{"}}{s_k} \tag{17}$$

$$a_{ik}=\frac{a_{ik}^{'}}{r_i} \tag{18}$$

Where r is the column vector of the m row-sums of A'.

3.1.4. Selection of Initial Polytope

The extended method of Full et.al. (1981) is employed to establish the initial polytope. The k most mutually extreme samples in the dataset are selected as vertices (the EXRAWC subroutine, Klovan and Miesch, 1976). For each of the first k factors of A'', EXRAWC selects the k samples with maximum loadings to form a good candidate set. The loading matrix A'' is first varimax rotated, and then loadings with the maximum absolute value in each row of A'' are identified. The rows corresponding to the maximum loadings are then put into a new $k \times k$ matrix O_0. Duplication is not allowed, which means there are no two identical rows in O_0. These k samples that make up matrix O_0 are the most mutually extreme samples. The PVA algorithm uses the k vectors as oblique reference axes for all samples. The resultant oblique loading matrix A_0'' and score matrix F_0'' are calculated as follows:

$$F_0'' = O_0 F'' \tag{19}$$

$$A_0'' = A'' O_0^{-1} \tag{20}$$

Matrices A_0'' and F_0'' are then scaled back to measurement space using the scaling functions described last section to yield A_0 and F_0.

Matrix A_0 is then inspected to determine if the k samples in O_0 are indeed the most mutually extreme. If the maximum loading values in A_0 equals 1 and correspond to

the samples taken from matrix O_0, then this O_0 is accepted as the final O_0. If the maximum loading values in A_0 are greater than 1, then the corresponding sample in $A^{"}$ is then taken to substitute that one was placed in O_0 before. If there is no matrix O_0 that can make the maximum loading values in A_0 less than or equal to 1, the initial O_0 is taken to do the following calculations.

3.1.5. DElete NEGatives (DENEG)

After determination of the initial polytope, the next step is to adjust the polytope so that both the fractions and the endmembers fall in a realistic value range. The DENEG subroutine first scans loading matrix A_0 and score matrix F_0 for adjustable negative values. There are three user-defined numerical criteria to distinguish between adjustable and nonadjustable negative values. First, the cutoff criterion for mixing proportions, t_1. Typically the default t_1 is -0.05, which means that a -5% mixing proportion in any sample is allowed. The second criterion t_2 is -0.25, referred as the DENEG value. The adjustable negative values of mixing proportions should be fall in the range between t_1 and t_2. The effect of t_2 is to prevent the algorithm iterating in an attempt to fit outlier into the model. Finally, the third criterion t_3 is the endmember composition cutoff criterion for the score matrix F_0. The value of t_3 is -0.05, and its purpose is to allow some noise in the model. If there are no adjustable negative values

both in A_0 and F_0, the DENEG subroutine stops. A_0 and F_0 are taken as the mixing proportion matrix and endmember composition matrix separately.

If there is adjustable negatives in A_0 and F_0, the DENEG procedure starts. DENEG is a process that alternates between solving A according by a nonnegative F and solving F according by a nonnegative A. This procedure iterates until both the mixing proportions and the endmember compositions have no adjustable negative values, or the algorithm meets the maximum iteration number set by the user.

Geometrically, the DENEG approach is a procedure of alternate polytope expansion and rotation. It begins by constructing an initial polytope in principle component space. As it mentioned above, the initial polytope is defined by selecting the most mutually extreme samples in the dataset as the initial vertices. If pure endmembers occur in the dataset, then DENEG's nonnegative criteria will be met on the first iteration. Otherwise, if there are negative adjustable values in the loading matrix A_0, the DENEG subroutine will begin a series of iterations to adjust A and F until neither matrix contains negative values.

DENEG first defines a $1\times k$ row vector D, in which elements d_i ($i=1,2,...k$) are the absolute value of lowest adjustable values in columns $i=1,2,...k$ of matrix A_0. A scalar z is then defined as:

$$z=\frac{1}{(1+d_1+d_2+...+d_n)} \tag{21}$$

Matrix $A_1 = \{a_{1ij}\}$ can be then calculated as:

$$a_{1ij} = (a_{0ij} + d_j) \times z \tag{22}$$

The resultant matrix A_1 is the endmember mixing proportions matrix without adjustable negative values. Geometrically, the effect of equation 22 is to move the edge of the polytope out in an edge parallel direction, and stop at the outermost sample from that edge. The corresponding loading matrix F_1 can be then calculated by matrix regression as:

$$F_1 = (A_1^T A_1)^{-1} A_1^T \hat{X} \tag{23}$$

Matrix F_1 represents the endmember compositions matrix. DENEG then scans F_1 for adjustable negative values using the criterion t_3. If there are no elements in F_1 less than t_3, DENEG stops iterating. A_1 is taken as the final mixing fractions and F_1 is taken as the final source compositions. However, if there are adjustable negatives in F_1, the algorithm continues to conduct the polytope rotation.

If there are adjustable negative values in F_1, the algorithm substitutes all the negatives with zeros. A new matrix F_2 is then defined by renormalizing each row in nonnegative F_1 to be sum to 100%. Then the previous described transformation is used to transfer F_2 into F_2''. A_2'' can be determined by matrix regression, and a new $k \times k$

oblique matrix O_2 can be extracted from using the method mentioned in section 3.1.4. Oblique scores and loadings matrices are then calculated as:

$$F_2'' = O_2 F'' \tag{24}$$

$$A_2'' = A'' O_2^{-1} \tag{25}$$

Matrix A_2'' is then scaled back to A_2 in the measurement space using the scaling function introduced in section 3.1.3. Matrix A_2 is then inspected for adjustable negative values. If no adjustable negative values are encountered in A_2, DENEG stops iteration. A_2 can be accepted as the final fraction matrix and F_2 as the final endmember composition matrix. However, if there is adjustable negative value in A_2, the program continue iterates. The algorithm redefines A_2 and F_2 as A_0 and F_0, and DENEG iterates from the beginning. A maximum iteration number is set in case of the iterations do not converge. Iterations will continue until there are no adjustable values in both matrices or the maximum iteration number is achieved.

3.2. PVA Applied on MODIS Reflectance

Dobreva et al. (2011) developed a method to map the snow fractions using Artificial Neural Network (ANN). This newly developed machine-learning model was trained, tested and validated using both Landsat and MODIS data. The data used in Dobreva et al. (2001) was also utilized in this study to develop the proposed PVA algorithm, and to

ensure the comparability when evaluating the its performance on fractional snow cover mapping with ANN and MODIS snow products.

3.2.1. MODIS Preprocessing

MODIS is a global environmental monitoring instrument aboard NASA's Terra and Aqua satellites. MODIS acquires images from every location on Earth once every 1 or 2 days in 36 discrete spectral bands (Barnes et al., 1998). A variety of standard products of MODIS data have been developed and are distributed free of charge. MOD09 is the MODIS surface reflectance product that computed from the MODIS Level 1B land bands 1 – 7 (modis.gsfc.nasa.gov). The seven estimated land surface reflectance bands at 500 m spatial resolution were used in the study and it can be downloaded at the Land Processes Distributed Active Archive Center: https://lpdaac.usgs.gov. Table 1 shows the 7 input bands to the PVA algorithm.

The datasets in the MOD09 product are provided in the MODIS sinusoidal projection. In this study, it was re-projected to a UTM projection with a WGS84 datum to match the reference snow maps.

Table 1. Input MODIS bands to PVA

Input MODIS Bands	Description
MOD09 Band 1	Reflectance in the red portion of the electromagnetic spectrum (620-670 nm)
MOD09 Band 2	Reflectance in the near infrared portion of the electromagnetic spectrum (841-876 nm)
MOD09 Band 3	Reflectance in the blue portion of the electromagnetic spectrum (459-479 nm)
MOD09 Band 4	Reflectance in the green portion of the electromagnetic spectrum (545-565 nm)
MOD09 Band 5	Reflectance in the shortwave infrared portion of the electromagnetic spectrum (1230-1250 nm)
MOD09 Band 6	Reflectance in the shortwave infrared portion of the electromagnetic spectrum (1628-1652 nm)
MOD09 Band 7	Reflectance in the shortwave infrared portion of the electromagnetic spectrum (2105-2155 nm)

3.2.2. Landsat Processing

Landsat ETM+ scenes were used for selecting random sample points as reference fractional snow cover. The images was obtained free of charge from the United States Geological Survey (USGS) Earth Resources and Observation and Science (EROS) data center. The Landsat images were classified into eight classes by combining the seventeen IGBP classes (Figure 2). Each of the Landsat ETM+ images was used as input to a snow cover mapping algorithm (Hall et al., 1995). This method identifies each pixel is snow or not and it was used for creating the MOD 10 product. The 30-m resolution binary snow maps were than used to calculate the corresponding fractions for each MODIS pixel, which was then used as a reference snow cover fraction in the following study.

Table 2. Land-cover classes used in this research

IGBP Land-cover Classes	Reclassified for Sampling
Evergreen needleleaf forest	Evergreen forests
Evergreen broadleaf forest	
Deciduous needleleaf forest	Deciduous forests
Deciduous broadleaf forest	
Mixed forests	Mixed forests
Croplands	Mixed agriculture
Urban and built-up	
Cropland/natural vegetation mosaic	
Barren/sparsely vegetated	Barren/sparsely vegetated
Woody savannas	Savannas
Savannas	
Closed shrublands	Grasslands/shrublands
Open shrublands	
Grasslands	
Permanent wetlands	Wetlands
Permanent snow and ice	N/A
Water	N/A

4. RESULTS

The Python PVA code was first tested against existing PVA code using known mixtures of Polychlorinated Biphenyls (PCBs) from Murphy and Morrison (2007) to ensure its correct operation. Then the PVA code was applied on MODIS spectral reflectance. In this analysis 25,467 random points from eight scenes with a wide range of snow fractions (0 - 1) and over different land cover types were selected to evaluate the performance of PVA. This observations are the same that were used in the Dobreva and Klein (2011) study. The snow fractions, calculated from corresponding Landsat imagery, were used as references to examine the precision of PVA computed FSC.

4.1. PVA Code Accuracy Applied on PCB Data

The Python PVA code was developed and tested against the existing code applied on known mixtures of PCBs. The results were presented in Figures 1 and 2. Figure 1 shows the estimated fractions both from Python PVA (red) and existing code (green). The overall difference between Python developed PVA code and existing code is 1.29×10^{-4}, which indicates that the developed Python code yield a quite similar estimate of fractions for the PCB data, compared to the existing code. Figures 2(a) through 2(c) illustrate the source compositions derived from the developed Python PVA code (red) and the existing code (green), respectively. Endmember 2 shows an exactly same pattern of source composition from developed Python code with the existing one, while the endmember 1 and 3 reveal a nearly same pattern between existing code and this implementation providing confidence of the success of our Python version of PVA

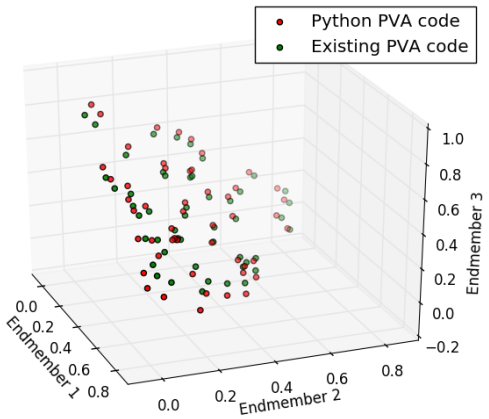

Figure 1. Comparison between fractions estimated from Python PVA code and the existing code

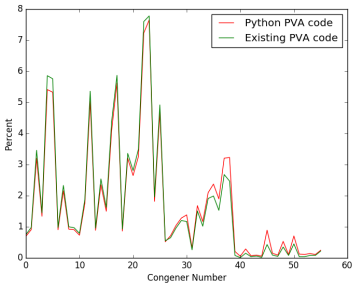

(a). Endmember 1

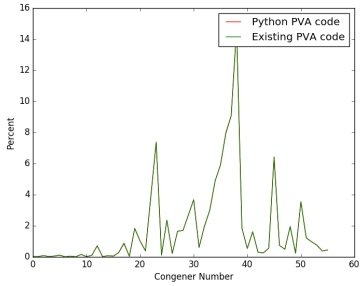

(b). Endmember 2

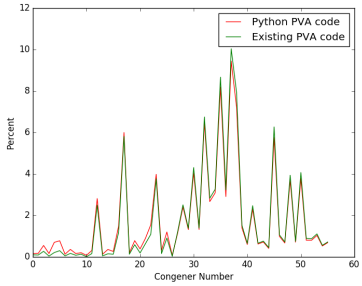

(c). Endmember 3

Figure 2. Endmembers derived from PCB data

4.2. Fractional Snow Cover Mapping

After testing the Python developed PVA codes' correctness using PCBs data, the Python codes were then applied on MODIS reflectances, as described in section 3.6. The MODIS, and corresponding Landsat images were collected from North America and are illustrated in Figure 3.

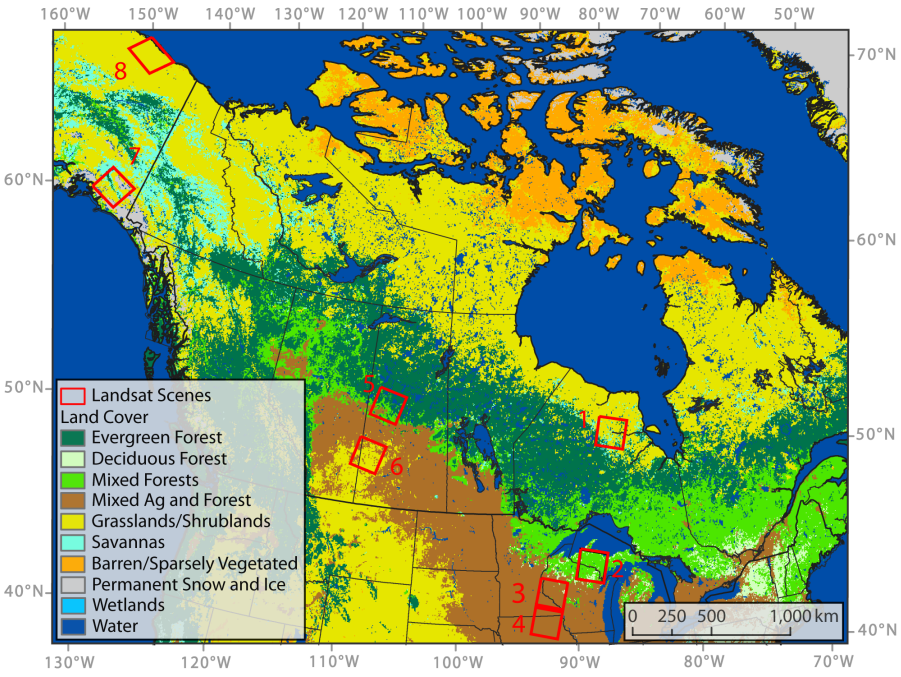

Figure 3. Scenes collected in this study. The basemap illustrates landcover classes for the scenes used in the study (Dobreva and Klein, 2011)

The Landsat data and corresponding MODIS data collected for this study is showed in Table 1 (produced by Dobreva). Nine Landsat scenes, and corresponding

MODIS scenes from the year 2000 to the year 2003 were selected with the geographical locations as Figure 3 presents.

Table 3. MODIS/Landsat scenes collected (Dobreva and Klein, 2011)

Scene	Path	Row	UTM	Year	Day_Number	MODIS_h_v
1	24	23	16	2000	115	1203
2	24	28	16	2002	344	1104
3	26	29	15	2002	38	1104
4	26	30	15	2002	38	1104
5	38	22	13	2003	77	1103
6	39	22	13	2002	305	1103
7	39	24	12	2002	305	1103
8	65	17	7	2001	132	1102
9	73	11	6	2002	143	1202

The utility of applying PVA to map fractional snow cover was investigated in the most generalized way possible. All MODIS/Landsat pairs from the Dobreva and Klein (2011) study from were analyzed simultaneously to determine endmember composition and fraction with the exception of Landsat scene 5, which was deemed problematic. Thus, this study should be viewed as perhaps the most difficult test of PVA applied to snow cover mapping. It would be expected that refining PVA to operate in on smaller geographic regions or tailored to individual land cover types would result in improved mapping. However, this research examines PVA as a parsimonious global snow mapping approach requiring no prior training.

As described in section 3.1.2, 95% was used as a threshold to select the appropriate number of eigenvalues to retain while employing PCA to reduce the overall dimensionality of the dataset. Figure 4 shows the cumulative percentage variance along principle components. The first three components explain 95.7049% of the overall variance of the dataset which. Therefore these three components were retained to in performing the PVA

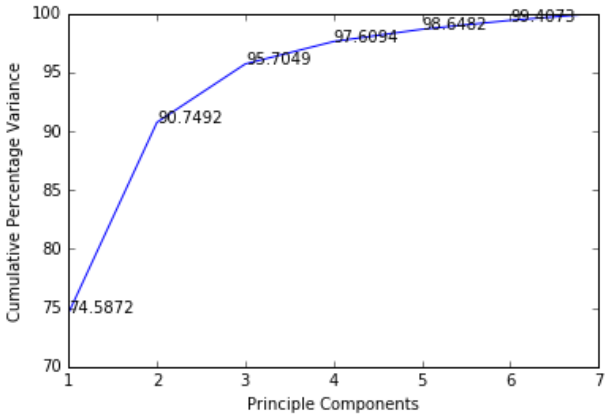

Figure 4. Cumulative percentage variance along principle components

The PVA derived endmembers for all samples from North America is illustrated in Figure 5. Through comparing the reflectance pattern over wavelength with the standard reflectance pattern of different land cover, the land cover type of each endmember can be inferred. Endmember one is snow, while endmember two is vegetation while endmember three appears to represent perhaps bare soil.

The fractions of endmember one were taken to represent the fraction of snow in each pixel. These were then was compared with the reference FSC calculated from Landsat (Figure 5) to determine overall snow mapping accuracy. The R^2 is 0.6294, indicates a reasonable good agreement between the MODIS FSC and Landsat reference. To better illustrate the comparison, the mean MODIS FSC was computed for five percent snow fraction bins and the mean and one standard deviation was plotted. Snow fractions were binned in intervals of five percent and plotted in Figure 6. It can be seen from the figure that PVA over-estimated the FSC for the pixels with low FSC value, while it under-

estimated the pixels with high FSC value. The maps showed from Figure 6(a) to Figure 6(c) show the spatial variability of PVA-derived FSC, Landsat FSC and the difference between them, for one of the eight selected Landsat scenes (path 24/row 23), mixed agriculture, barren/sparsely vegetated, and savannas.

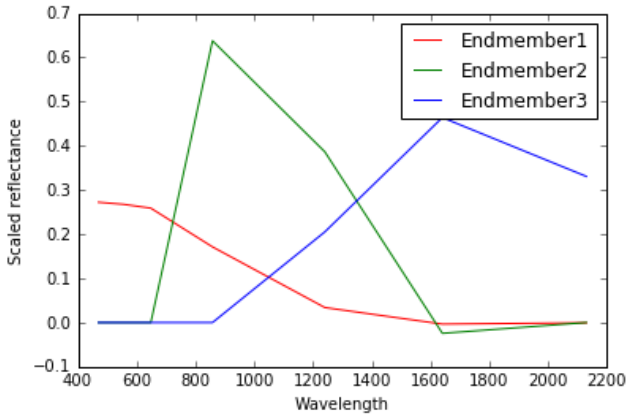

Figure 5. PVA derived source composition from MODIS reflectance

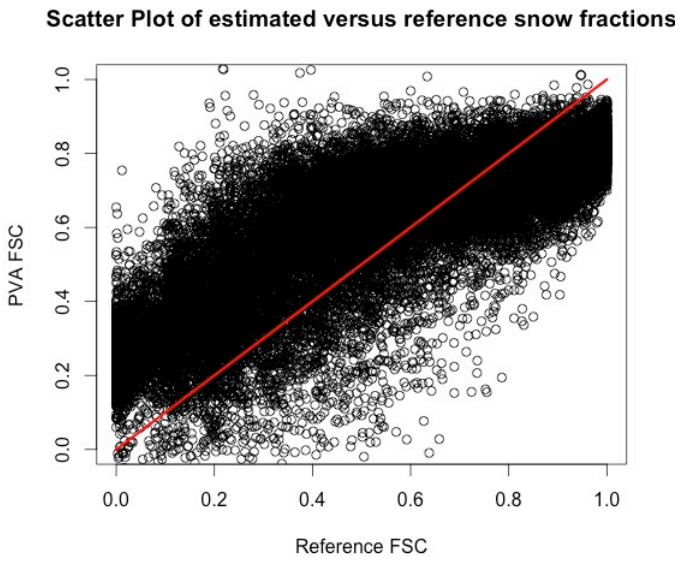

Figure 6. Scatter plot of test 8 scenes

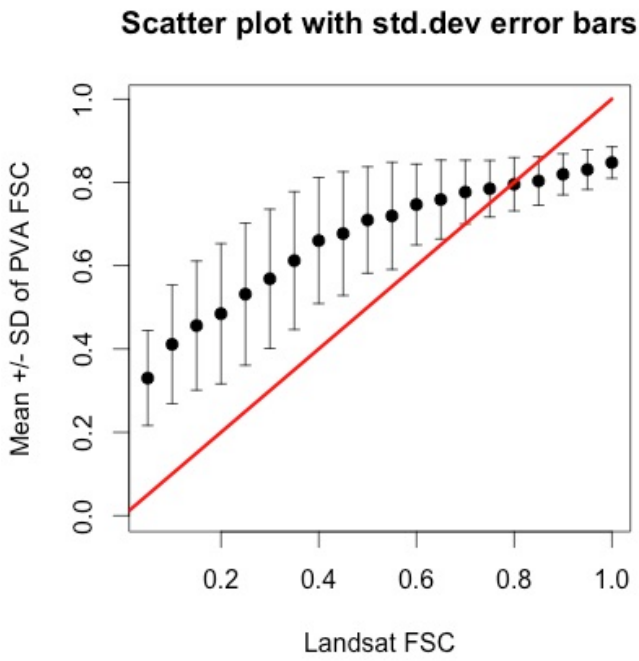

Figure 7. Error bar of PVA derived FSC vs. reference FSC

The Root Mean Square Error (RMSE) was also calculated to examine the mapping accuracy of PVA. RMSE was computed as

$$RMSE = \sqrt{\frac{1}{1-n} * \sum_{i=1}^{n} (x' - x)^2} \tag{26}$$

where n is the number of samples, x' is the estimated FSC from PVA and x is the reference FSC from Landsat. The RMSE for the eight Landsat scenes is 0.1286.

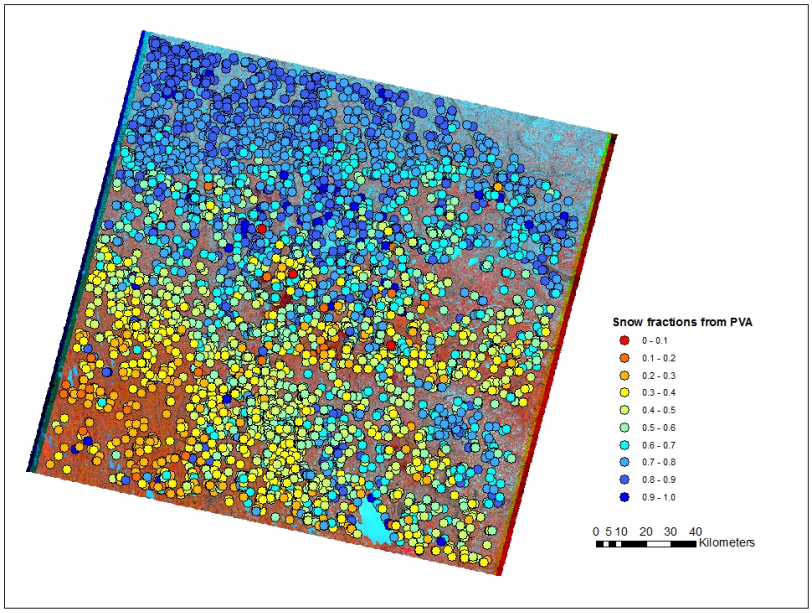

(a). Snow map derived from PVA Landsat scene path 24/row 23 on 4/24/2000

Figure 8. Snow maps for Landsat scene path 24/row 23 on 4/24/2000

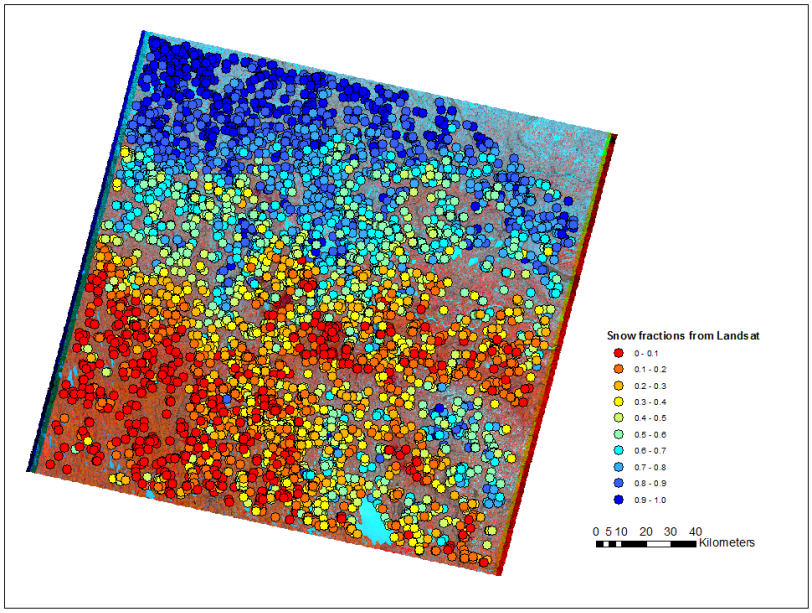

(b). Snow map derived from Landsat image for Landsat scene path 24/row 23 on 4/24/2000

Figure 8. Continued

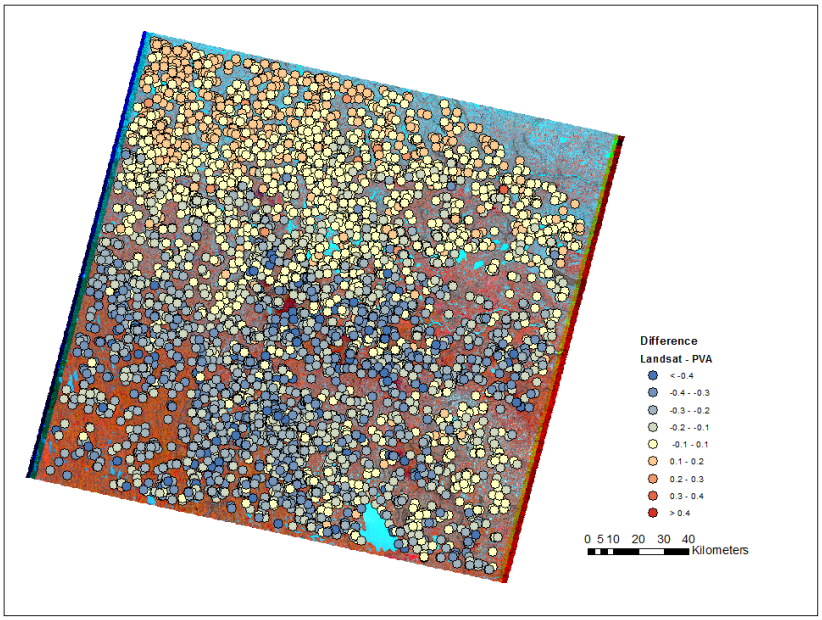

(c). Difference between snow fractions estimated from PVA and Landsat for Landsat scene path 24/row 23 on 4/24/2000

Figure 8. Continued

4.3. Mapping Accuracy by Land Cover

The mapping accuracy of PVA was also examined by land cover. Both R^2 and RMSE were calculated to evaluate the PVA performance on different land cover type. Figure 7 illustrates the scatter plots of PVA estimated FSC versus the reference Landsat FSC over different land covers. Table 3 lists the R^2 and RMSE value for each land cover category. The barren/sparsely vegetated class has the largest R^2 of 0.75, but has a

relatively small RMSE of 0.08. The wetland class has the smallest RMSE of 0.05 but a relatively small R^2 of 0.54 indicates a poor fit.

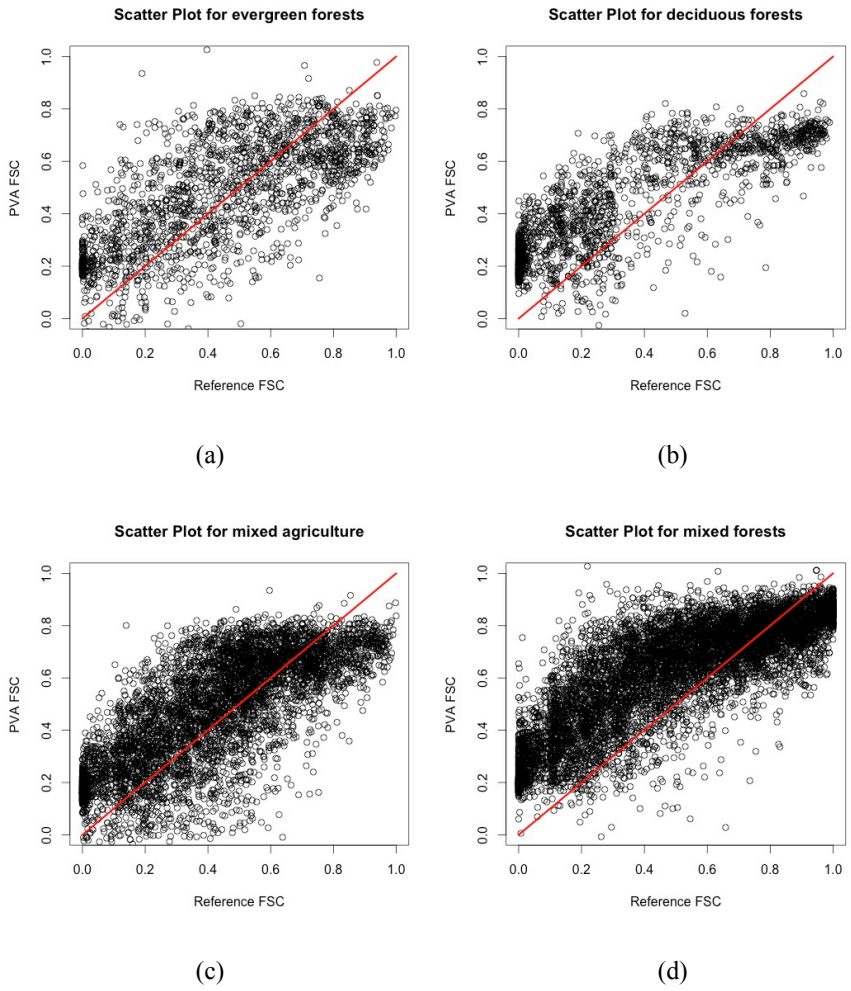

Figure 9. Scatter plot by land-cover: (a). Evergreen forests, (b). Deciduous forests, (c). Mixed agriculture, (d). Mixed forests, (e). Barren/sparsely vegetated, (f). Savannas, (g). Grasslands/shrublands, (h). Wetlands

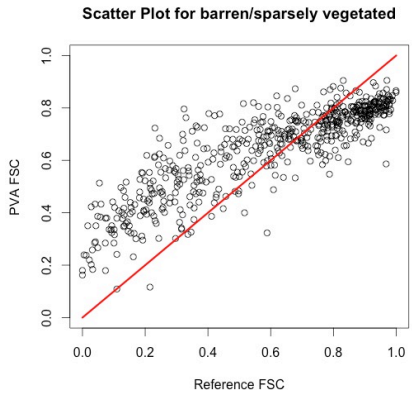

(e)

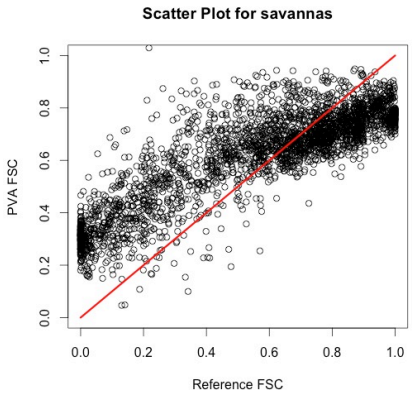

(f)

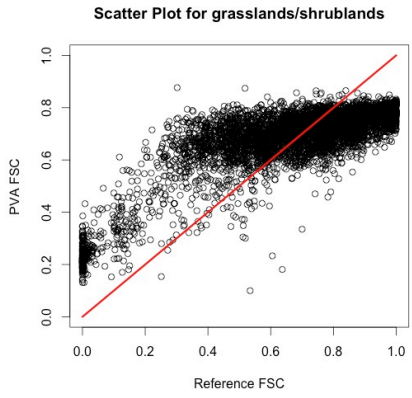

(g)

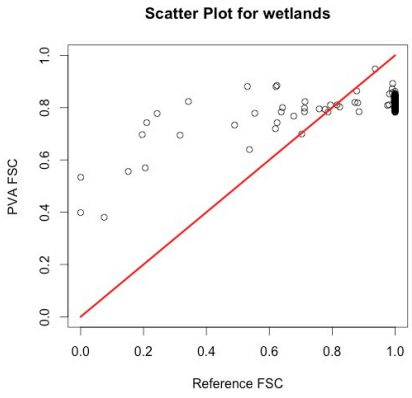

(h)

Figure 9. Continued

Table 4. R^2 **and RMSE by land-cover of different methods (Dobreva and Klein, 2011)**

	PVA		MOD10 FSC		MOD10 binary		ANN[a]		ANN[b]	
Landover	R^2	RMSE	R^2	RMSE	R^2	RMSE	R^2	RMSE	R^2	RMSE
Evergreen forests	0.50	0.15	0.77	0.19	0.29	0.52	0.82	0.15	0.79	0.16
Deciduous forests	0.68	0.11	0.90	0.11	0.61	0.36	0.94	0.09	0.92	0.10
Mixed forests	0.55	0.14	0.82	0.14	0.46	0.47	0.87	0.12	0.80	0.15
Mixed agriculture	0.63	0.12	0.68	0.12	0.37	0.21	0.74	0.11	0.73	0.12
Barren/sparsely vegetated	0.75	0.08	0.90	0.15	0.86	0.18	0.92	0.13	0.91	0.14
Savannas	0.72	0.09	0.87	0.15	0.52	0.39	0.92	0.12	0.91	0.12
Grasslands/shrublands	0.65	0.08	0.90	0.13	0.78	0.23	0.94	0.11	0.93	0.12

[a] ANN where land cover was input as 1 categorical variable (1LC)
[b] ANN where land cover was input as 16 binary variables (16LC)

5. DISCUSSION

5.1. Overall Performance of PVA

Given that this research took the most parsimonious approach by developing a single PVA model for all the MODIS observations acquired from across North America used in Dobreva and Klein (2011), the overall performance of PVA was considered to be good. PVA successfully identified three major endmembers and was able to estimate the snow fraction in each pixel based on a single identified snow endmember from the reflectance of seven MODIS bands as inputs.

Agreement between the PVA derived FSC and the reference Landsat FSC with R^2 of 0.6294 and RMSE of 0.1286 is illustrated in Figure 4. This is an acceptable result given that all the heterogeneity in the North American landscape was modelled by three oblique endmembers. In addition, the PVA method has never been applied in the field of snow mapping before.

As can be seen in Figures 4 -7, there is a strong non-linearity in the relationship between the MODIS PVA estimated and the Landsat reference FSC f. PVA tends to estimate FSC for pixels with low snow fractions and underestimates FSC for pixels with high snow fractions. As it can been seen from the scatter plot and error bar plot (Figure 4 and 5), snow fractions less than 0.6 tend to be overestimated and the standard deviation is larger in this range, while the snow fractions larger then 0.6 tend to be underestimated but have a smaller deviation in the estimated snow cover fractions.. It appears for most landcovers (Figure 7) the PVA estimated FSC increases linearly compared to the

Landsat reference, though not necessarily along the 1:1 line at lower snow fractions while the PVA estimates tend to level off at approximately 80% while Landsat reference snow cover fractions continue to increase. This behavior can also be seen in the Dobreva and Klein (2011) artificial neural network (ANN) estimates of snow cover fractions from MODIS.

The computed source composition shown in Figure 3 illustrates that the PVA method can decompose the general endmember pattern for samples collected across all of North America fairly reasonably, even when limiting the analysis to three eigenvalues It can be seen from Figure 3 that the pattern of endmember 1 is similar as snow, as it dramatically decreases at the near infrared region of the electromagnetic spectrum, and endmember 2 is vegetation, as its reflectance increases dramatically in the near infrared spectrum. However, the reflectance s differ between from the standard spectral reflectance for the snow. The standard reflectance of snow can be up to 100% at the visible portion region of the electromagnetic spectrum while the PVA computed values appear to have maximum reflectances in the visible of only 30%. The reason for this is related to the data transformation process. The original mixed spectral data was transformed to constant row-sum data, but is no effective way to transfer the constant row-sum data back to the original scalar.

5.2. Comparison to the Standard MODIS Snow-Cover Product

The PVA derived FSC was also compared with the MOD10 product (Riggs et al, 2006). The MOD10A1 product provides both the fractional snow cover and binary snow cover products. Dobreva and Klein (2011) conducted experiments on Artificial Neural

Network (ANN) for fractional snow cover mapping and evaluated its performance by comparison with MOD10 snow product. The results are shown in Tables 4 and 5. Although the number of samples differs between this study and the Dobreva and Klein (2011) study as the ANN required considerable number of samples for training the study areas and Landsat scenes used are the same. The R^2 of MOD10 FSC is 0.87, and the R^2 of MOD10 binary is 0.53, while the R^2 of PVA is 0.63. The performance of PVA is comparable with both the MOD10 FSC and binary product based on the correlation between the estimated and reference snow fractions. However, the performance of MOD10 FSC is a better than PVA, while PVA performs better than MOD10 binary product. In terms of RMSE, MOD10 FSC has a 0.13 RMSE, and MOD10 binary has 0.33, while PVA has 0.13, identical to MOD10 FSC. It appears that the PVA method can achieve similar FSC accuracy as measured by RMSE when compared to the reference Landsat snow maps and did not require development of an empirical linear relationship between FSC and NDSI

Table 4 shows the work done by Dobreva and Klein (2011), they compared the performance of ANN with MOD10 FSC and MOD binary product per land cover as well. Based on their work, the PVA accuracy by land cover was also examined. By comparing Table 3 to Table 4, it can be seen that the magnitude of RMSE from PVA is comparable to that of MOD10 FSC, while the RMSE from MOD10 binary is much different. The comparable RMSE between PVA and MOD10 FSC demonstrates the similar measurement accuracy between both methods. For the R^2, MOD10 FSC has the largest R^2 of all the land cover type, while PVA has the second largest value over

MOD10 Binary, except for the barren/sparsely vegetated and grasslands/shrublands land covers. This result reveals that the MOD10 FSC has the best agreement with reference, following the PVA, which is identical with the overall accuracy evaluation. For each different land cover, all of the three products have the smallest R^2 in the class of evergreen forests and the largest R^2 in the class of barren/sparsely vegetated. The similar trend in R^2 of these three methods to some extent demonstrates the difficulty in unmixing snow from evergreen forest.

5.3. Comparison to ANN

The FSC derived from PVA was also compared with that computed from ANN (Dovreva and Klein, 2011) to evaluate the performance of PVA. In this research, ANN was operated twice using land cover as different inputs for each time. When land cover was input as a single categorical variable, the R^2 is 0.90 and RMSE is 0.12. When land cover was input as 16 binary variables, the R^2 is 0.89 and RMSE is 0.13. Only slightly difference was existed between these two methods. Comparing with PVA's R^2 of 0.63 and RMSE of 0.13, ANN presents a better agreement with the reference Landsat data. However, PVA has a nearly same RMSE with ANN, which shows the similar measure accuracy with ANN. The advantage of PVA is that it performance required no extensive training dataset as was required by the ANN approach.

Table 4 presents the R^2 and RMSE of ANN applied on different land covers (Dobreva and Klein, 2011). Two methods as illustrated before were used to run ANN. Similar as the overall accuracy; the accuracy difference per land cover between these two methods was found to be small. ANN has the largest R^2 in the class of

grasslands/shrublands while PVA has its largest value in barren/sparsely vegetated, while they both have smallest R^2 in the class of evergreen forests, which indicates the difficulties in accurately mapping fractional snow cover in forests. The R^2 of ANN in each land cover is larger than that of PVA, which shows a better performance of estimation of snow fraction, but PVA shows a similar RMSE with ANN, which demonstrated a comparable measure accuracy.

Although PVA has lower R^2 than both the MOD10 FSC product and ANN when comparing with the reference Landsat data, the comparable RMSE demonstrated the ability and potential in application of PVA in fractional snow mapping. Unlike ANN, the PVA was not trained in any way. In this study, only three endmembers were retained after conducting the dimensionality deduction. Comparing the inputs used in ANN, including 7 MODIS bands, NDVI, NDSI and land cover types, PVA has a much smaller input dataset but achieved the comparable results. This high generalization of PVA may be the reason why its agreement with reference is not as good as the other methods, but the comparable R^2 and RMSE demonstrated its potential in application in fractional snow cover mapping.

5.4. Mapping Accuracy by Land Cover

The accuracy of PVA derived snow fractions were also examined by land cover. The FSC estimated from these eight land cover types, including evergreen forests, deciduous forests, mixed agriculture, mixed forests, barren/sparsely vegetated, savannas, grasslands/shrublands and wetlands were compared with the reference Landsat FSC

separately. R^2 and RMSE were calculated to evaluate the performance of PVA over different land covers.

As Table 4 presents, evergreen forests have the lowest R^2 of 0.5 and the largest RMSE of 0.15, following by the wetlands with R^2 of 0.54 and RMSE of 0.05. The reason that the wetlands have the smallest RMSE may because there are many fewer observations in this class type than in the others. The evergreen forests with lowest R^2 and largest RMSE indicating the performance of PVA applied on to evergreen forests is not as good as on the others. However, it is accordant with the results from some other snow mapping research (Klein et al., 1998). It is because the forests create complicated shading on the forest floor and can obscure snow-covered ground from the sensor especially at high sensor zenith angles. Therefore, the reflectance MODIS collected from that specific area may not detect all the snow present on the ground. On the other hand, the barren/sparsely vegetated land cover has the highest R^2 of 0.75 and a relatively small RMSE of 0.08, which indicates a quite good performance of PVA on for areas with sparse vegetation.

In summary, PVA estimated the snow fractions successfully given the high level of simplification on the input data set. In this study, the PVA retained only three principal components while the input data set has seven dimensionalities, which generalized all the land cover types over North America into three categories. However, as the above sections described, both the overall mapping accuracy and the accuracy by land cover showed a consistent trend between PVA and ANN, as well as MOD10 product when estimating the fractional snow cover. Spatially (Figure 8), PVA can

capture the pattern of distribution of snow fractions although not as much as variability as the reference, which is also evidenced by the low R^2. This low R^2 couldn't demonstrated that the PVA has a poor performance on estimating snow fractions, since it utilized only limited information from the input data set, yet it presented the consistency both statistically and spatially with other methods (ANN and MOD10) that use more information than PVA does, in estimating the snow fractions. Therefore, PVA did achieve its success in deriving snow fractions with simplification of input data.

6. CONCLUSIONS AND FUTURE DIRECTIONS

In this study, a Polytopic Vector Analysis (PVA) algorithm was first implemented in Python and tested against the existing code by using the known PCBs data. The developed Python code showed a good performance on the PCBs data and the correctness of the PVA algorithm was approved. Then the PVA algorithm was applied on the MODIS reflectance to unmix the source composition and fraction of snow covered pixels from North America. Seven MODIS bands were used as input and the output snow fractions were compared with the Landsat reference snow fractions, both over the whole testing data and over the different land covers separately.

The PVA algorithm showed a good performance on snow fractions mapping and a potential to be applied on other types of land cover mapping. It shows a good agreement of the estimated snow fractions comparing with the reference derived from Landsat imagery. Although its accuracy is not as good as other fractional snow cover mapping method, such as ANN, the PVA still showed the potential to be applied not only on snow mapping, but also other land cover mapping. It can decompose a pixel into different land cover, and the lancover type can be determined by comparing the computed source composition reflectance pattern with the standard land cover reflectance.

This is the first study to apply the PVA method to mapping snow-covered fractional snow mapping study. It illustrates the feasibility of PVA algorithm in dealing with mixing reflectance of satellite imagery. Future efforts will be put into the aspects

that include: 1) improving the PVA algorithm by adjusting the procedure for MODIS reflectance analysis, and by developing a larger dataset; 2） developing a more sophisticated algorithm in addition to PVA algorithm, for example, including the NDSI or NDVI indices as input to the PVA procedure. 3) applying the PVA algorithm on specific land cover types, and 4) evaluating its performance by comparing the results to other fractional snow cover mapping approaches.

REFERENCES

Appel, I. L., V. V. Salomonson, Ieee & I. Ieee (2002) Estimate of fractional snow cover using MODIS data. *Igarss 2002: Ieee International Geoscience and Remote Sensing Symposium and 24th Canadian Symposium on Remote Sensing, Vols I-Vi, Proceedings: Remote Sensing: Integrating Our View of the Planet***,** 3044-3046.

Arnfield, A. J. (2006) Micro-and mesoclimatology. *Progress in Physical Geography,* 30**,** 677-689.

Barnett, T. P., J. C. Adam & D. P. Lettenmaier (2005) Potential impacts of a warming climate on water availability in snow-dominated regions. *Nature,* 438**,** 303-309.

Brown, R. D. & P. W. Mote (2009) The response of Northern Hemisphere snow cover to a changing climate. *Journal of Climate,* 22**,** 2124-2145.

Cherry, J. E., L. Tremblay, M. Stieglitz, G. Gong & S. Déry (2007) Development of the pan-arctic snowfall reconstruction: New land-based solid precipitation estimates for 1940–99. *Journal of Hydrometeorology,* 8**,** 1243-1263.

Chokmani, K., N. Yawu Sena, E. Gloaguen & M. Bernier. 2013. Multi-scale analysis of the spatial variability of the snow water equivalent (SWE) over Eastern Canada. In *EGU General Assembly Conference Abstracts*, 5649.

Dobreva, I. D. & A. G. Klein (2011) Fractional snow cover mapping through artificial neural network analysis of MODIS surface reflectance. *Remote Sensing of Environment,* 115**,** 3355-3366.

Dozier, J. (1989) Spectral signature of alpine snow cover from the landsat thematic mapper. *Remote Sensing of Environment,* 28**,** 9-&.

Full, W. E., R. Ehrlich & J. C. Bezdek (1982) Fuzzy-Qmodel - a new approach for linear unmixing. *Journal of the International Association for Mathematical Geology,* 14**,** 259-270.

Full, W. E., R. Ehrlich & J. E. Klovan (1981) Extended Qmodel - Objective definition of external end members in the analysis of mixtures. *Journal of the International Association for Mathematical Geology,* 13**,** 331-344.

Hall, D. K., G. A. Riggs & V. V. Salomonson (1995) Development of methods for mapping global snow cover using moderate resolution imaging spectroradiometer data. *Remote Sensing of Environment,* 54**,** 127-140.

Hall, D. K., G. A. Riggs, V. V. Salomonson, N. E. DiGirolamo & K. J. Bayr (2002) MODIS snow-cover products. *Remote sensing of Environment,* 83**,** 181-194.

Jensen, J. R. (2005) Introductory digital image processing: A remote sensing perspective (3rd ed.). *Pearson College Division*.

Johnson, G. W. a. G. D. N. (1998) Unmixing of AVIRIS hyperspectral data from Dixie Valley, Nevadaî. *Proceedings: Twenty-Third Workshop on Geothermal Reservoir Engineering, Stanford University, Stanford, California,* 23**,** 240-245.

Klein, A. G., D. K. Hall & G. A. Riggs (1998) Improving snow cover mapping in forests through the use of a canopy reflectance model. *Hydrological Processes,* 12**,** 1723-1744.

Klovan, J. & J. Imbrie (1971) An algorithm and FORTRAN-IV program for large-scaleQ-mode factor analysis and calculation of factor scores. *Mathematical Geology,* 3**,** 61-77.

Klovan, J. E. & A. T. Miesch (1976) Extended cabfac and Qmodel computer programs for Q-mode factor analysis of compositional data. *Computers & Geosciences,* 1**,** 161-178.

Koskinen, J. T., J. T. Pulliainen & M. T. Hallikainen (1997) The use of ERS-1 SAR data in snow melt monitoring. *IEEE Transactions on geoscience and remote sensing,* 35**,** 601-610.

Manson, V. & J. Imbric. 1964. FORTRAN program for factor and vector analysis of geologic data using an IBM 7090/7094; Or 7094/1401 computer system. *State Geological Survey, University of Kansas*.

Mason, E. W. & R. Ehrlich (1995) Automated, quantitative assessment of basin history from a multiwell analysis. *Aapg Bulletin-American Association of Petroleum Geologists,* 79**,** 711-724.

Murphy, B. L., and Robert D. Morrison, eds. (2014) Introduction to environmental forensics. *Academic Press*.

Nash G D, J. G. W. (2002) Soil mineralogy anomaly detection in Dixie Valley, Nevada using hyperspectral data. *Twenty-Seventh Workshop on Geothermal Reservoir Engineering Stanford University, Stanford, California.* **,** 28-30.

Niu, G. Y. & Z. L. Yang (2007) An observation‐based formulation of snow cover fraction and its evaluation over large North American river basins. *Journal of Geophysical Research: Atmospheres,* 112.

Nolin, A. (2010) Recent advances in remote sensing of seasonal snow. *Journal of Glaciology,* 56**,** 1141-1150.

Nolin, A. W. & J. Dozier (1993) Estimating snow grain-size using aviris data. *Remote Sensing of Environment,* 44**,** 231-238.

Nolin, A. W. & J. Stroeve (1997) The changing albedo of the Greenland ice sheet: implications for climate modeling. *Annals of Glaciology, Vol 25, 1997: Papers from the International Symposium on Representation of the Cryosphere in Climate and Hydrological Models Held at Victoria, British Columbia, Canada, 12-15 August 1996,* 25**,** 51-57.

Painter, T. H., J. Dozier, D. A. Roberts, R. E. Davis & R. O. Green (2003) Retrieval of subpixel snow-covered area and grain size from imaging spectrometer data. *Remote Sensing of Environment,* 85**,** 64-77.

Painter, T. H., K. Rittger, C. McKenzie, P. Slaughter, R. E. Davis & J. Dozier (2009) Retrieval of subpixel snow covered area, grain size, and albedo from MODIS. *Remote Sensing of Environment,* 113**,** 868-879.

Painter, T. H., D. A. Roberts, R. O. Green & J. Dozier. 1997. Estimating snowcover and grain size from AVIRIS data with spectral mixture analysis and modeled snow spectra.

Pielmeier, C. & M. Schneebeli (2003) Stratigraphy and changes in hardness of snow measured by hand, ramsonde and snow micro penetrometer: a comparison with planar sections. *Cold Regions Science and Technology,* 37**,** 393-405.

Rango, A. (1993) Snow hydrology processes and remote-sensing .2. *Hydrological Processes,* 7**,** 121-138.

Rango, A. (1996) Spaceborne remote sensing for snow hydrology applications. *Hydrological Sciences Journal,* 41**,** 477-494.

Rango, A. & A. I. Shalaby (1998) Operational applications of remote sensing in hydrology: success, prospects and problems. *Hydrological Sciences Journal-Journal Des Sciences Hydrologiques,* 43**,** 947-968.

Rees, W. G. 2005. *Remote Sensing of Snow and Ice*. Taylor & Francis.

Robinson, D. A., K. F. Dewey & R. R. Heim (1993) Global snow cover monitoring - an update. *Bulletin of the American Meteorological Society,* 74**,** 1689-1696.

Roesch, A., M. Wild, H. Gilgen & A. Ohmura (2001) A new snow cover fraction parametrization for the ECHAM4 GCM. *Climate Dynamics,* 17**,** 933-946.

Romanov, P., D. Tarpley, G. Gutman & T. Carroll (2003) Mapping and monitoring of the snow cover fraction over North America. *Journal of Geophysical Research: Atmospheres,* 108.

Ross, D. (1997) Historical variability in Northern Hetnisphere spring snow-covered area.

Sabol, D. E., J. B. Adams & M. O. Smith (1992) Quantitative subpixel spectral detection of targets in multispectral images. *Journal of Geophysical Research: Planets,* 97**,** 2659-2672.

Salomonson, V. & I. Appel (2004) Estimating fractional snow cover from MODIS using the normalized difference snow index. *Remote sensing of environment,* 89**,** 351-360.

Schowengerdt, R. A. (1997) Remote sensing: Models and methods for image processing (2nd ed.). *San Diego, CA: Academic Press.*

Simpson, J. J. & T. J. McIntire (2001) A recurrent neural network classifier for improved retrievals of areal extent of snow cover. *Ieee Transactions on Geoscience and Remote Sensing,* 39**,** 2135-2147.

Simpson, J. J., J. R. Stitt & M. Sienko (1998) Improved estimates of the areal extent of snow cover from AVHRR data. *Journal of Hydrology,* 204**,** 1-23.

APPENDIX

Terminology and Abbreviations:

Artificial Neural Network (ANN): A machine learning method used by Dobreva and Klein (2011) for fractional snow cover mapping.

Fractional Snow Cover (FSC): The fraction of snow cover within one pixel of remote sensing imagery.

Normalized Difference Snow Index (NDSI): An index calculated between the visible reflectance and shortwave infrared reflectance to detect the presence of snow.

Normalized Difference Vegetation Index (NDVI): An index that normalizes between the near infrared reflectance and visible reflectance to detect the presence of vegetation.

Transformed loading (A''): Fractions of different land cover type obtained after principal component analysis of transformed MODIS reflectance (X'').

Loading (A): Fractions of different ground land cover type in measurement space, which is computed by the scaling function described in section 3.1.3.

Reflectance (X): Original reflectance data extracted from MOD09.

Reflectance after data transformation (X''): Reflectance transformed by equal vector length transformation.

Transformed score (F''): Source composition obtained after principle component analysis of transformed MODIS reflectance (X'').

Score (F): The source composition, which is reflectance of different land cover type at each MODIS band in this case.